

Submitted to the Editor of the Astrophysical Journal

A Magnetic Dynamo Origin For The Sub-mm Excess In Sgr A*

Fulvio Melia^{†1}, Siming Liu*, and Robert Coker^{††}

[†]Physics Department and Steward Observatory, The University of Arizona, Tucson, AZ
85721

*Physics Department, The University of Arizona, Tucson, AZ 85721

^{††}Department of Physics & Astronomy, The University of Leeds, Leeds LS2 9JT, UK

Received _____; accepted _____

¹Sir Thomas Lyle Fellow and Miegunyah Fellow.

ABSTRACT

The sub-mm bump observed in the spectrum of Sgr A* appears to indicate the existence of a compact emitting component within several Schwarzschild radii, r_S , of the nucleus at the Galactic Center. This is interesting in view of the predicted circularized flow within $\sim 5 - 10 r_S$, based on detailed multi-dimensional hydrodynamic simulations of Bondi-Hoyle accretion onto this unusual object. In this paper, we examine the physics of magnetic field generation by a Keplerian dynamo subject to the conditions pertaining to Sgr A*, and show that the sub-mm bump can be produced by thermal synchrotron emission in this inner region. This spectral feature may therefore be taken as indirect evidence for the existence of this circularization. However, the required accretion rate in the Keplerian flow is orders of magnitude smaller than that predicted by the Bondi-Hoyle simulations. We speculate that rapid evaporation, in the form of a wind, may ensue from the heating associated with turbulent mixing of gas elements with large eccentricity as they settle down into a more or less circular (i.e., low eccentricity) trajectory. The spectrum of Sgr A* longward of $\sim 1 - 2$ mm may be generated in the transition region outside of the Keplerian flow.

Subject headings: accretion—black hole physics—hydrodynamics—Galaxy: center—magnetic fields: dynamo—magnetohydrodynamics—plasmas

1. Introduction

The dark matter concentrated within the inner 0.015 pc at the Galactic Center has a measured mass of $2.6 \pm 0.2 \times 10^6 M_\odot$ (Genzel et al. 1996; Eckart & Genzel 1996; Eckart & Genzel 1997; Ghez et al. 1998). Most of it appears to be associated with Sgr A*, a bright, compact radio source (Balick & Brown 1974) that anchors the stars and gas locked in its vicinity, and provides possibly the most compelling evidence for the existence of supermassive black holes.

The spectrum of this unusual object can be described as a power-law with an index a that varies within the range $0.19 - 0.34$ ($S_\nu \propto \nu^a$) from cm to mm wavelengths. However, one of the most interesting features currently under focus is the suggestion of a sub-millimeter (sub-mm) spectral bump (Zylka et al. 1992; Zylka et al. 1995), since the highest frequencies appear to correspond to the smallest spatial scales (e.g., Melia, Jokipii & Narayanan 1992; Melia 1994; Coker and Melia 2000). In the case of Sgr A* one expects the sub-mm emission to come directly from the vicinity of the black hole. The existence of this bump (or “excess”) has been uncertain due to the variability of Sgr A*, but is now well established following a set of simultaneous observations (from $\lambda 20$ cm to $\lambda 1$ mm) using the VLA, BIMA, Nobeyama 45 m, & IRAM 30 m telescopes (Falcke, et al. 1998).

The behavior of Sgr A* is dictated by the manner with which plasma accretes onto it from the nearby environment. Three-dimensional hydrodynamic simulations of the gas dynamics at the location of Sgr A* (Coker & Melia 1997) indicate that the accreted specific angular momentum λ (in units of cr_S , where $r_S \equiv 2GM/c^2$ is the Schwarzschild radius in terms of the black hole mass M) can vary by 50% over $\lesssim 200$ years with an average equilibrium value for λ of 40 ± 10 . Thus, even with a possibly large amount of angular momentum present in the wind surrounding the nucleus, relatively little specific angular momentum is accreted. This is understandable since clumps of gas with a high specific

angular momentum do not penetrate to within the capture radius, $R_A \equiv 2GM/v_w^2$, defined in terms of the wind velocity v_w at infinity. The variability in the sign of the components of λ suggests that if an accretion disk forms at all, it dissolves, and reforms (perhaps) with an opposite sense of spin on a time scale of ~ 100 years.

The captured gas is highly ionized and magnetized, so it radiates via bremsstrahlung, cyclo-synchrotron and inverse Compton processes. However, this emissivity appears to be inefficient in the case of Sgr A*, so most of the dissipated energy within the large scale quasi-spherical inflow is carried inwards (Shapiro 1973; Ipser & Price 1977; Melia 1992). A viable explanation for Sgr A*'s low radiating efficiency is that the advected magnetic field is well below its equipartition value. This may not be surprising in view of the fact that the actual value of B depends strongly on the mechanism of field line annihilation, which is poorly understood. Two processes that have been proposed are (i) the Petschek (1964) mechanism, in which dissipation of the sheared magnetic field occurs in the form of shock waves surrounding special neutral points in the current sheets and thus, nearly all the dissipated magnetic energy is converted into the magnetic energy carried by the emergent shocks; and (ii) van Hoven's (1979) tearing mode instability, which relies on resistive diffusion of the magnetic field and is very sensitive to the physical state of the gas. In either case, the magnetic field dissipation rate is a strong function of the gas temperature and density, so that assuming a fixed ratio of the magnetic field to its equipartition value may not be appropriate.

Kowalenko & Melia (1999) have used the van Hoven prescription to calculate the magnetic field annihilation rate in a cube of ionized gas being compressed at a rate commensurate with that expected for free-fall velocity onto the nucleus at the Galactic Center. Whereas the rate of increase $\partial B/\partial t|_f$ in B due to flux conservation depends only on the rate \dot{r} of the gas, the dissipation rate $\partial B/\partial t|_d$ is a function of the state variables and

it is therefore not necessarily correlated with \dot{r} . Although these attempts at developing a physical model for magnetic field dissipation in converging flows is still rather simplistic, it is apparent from the test simulations that the equipartition assumption is not always a good approximation to the actual state of a magnetohydrodynamic flow, and very importantly, that the violation of equipartition can vary in degree from large to small radii, in either direction.

The first serious attempt at modeling the spectrum of Sgr A* using a sub-equipartition profile for the magnetic field was made by Coker & Melia (2000), who adopted a spherical infall as a simplified version of the actual accretion picture. Of course, the real accretion flow will deviate from radial at small distances from the black hole, where the gas begins to circularize with its advected specific angular momentum. This deviation of the accreting gas away from a purely radial infall may provide a clue for the appearance of the bump in the spectrum at sub-mm wavelengths, which seems to hint at the existence of a distinct geometry for the emitter at this energy. We here suggest that the sub-mm “excess” in the spectrum of Sgr A* may be the first indirect evidence for the anticipated circularization of the gas falling into the black hole at $5 - 25 r_S$. Although the physical conditions within the quasi-spherical infall evidently suppress the magnetic field well below its equipartition value, this need not be the case once the gas circularizes and forms a Keplerian structure. Indeed, it is expected that a magnetic dynamo within the differentially rotating region may overwhelm the field annihilation rate and actually lead to a saturated field intensity.

It is our intention here to fully explore the magnetic properties of this inner circulating region, and to assess the likelihood of producing the sub-mm spectral bump with a magnetic dynamo. Given the wide latitude of possible configurations in the outer quasi-spherical infall for producing the longer wavelength radio emission, we will not here attempt to construct a complete picture for the whole accretion region. Rather, this task is better

coupled to a hydrodynamic simulation that self-consistently merges the large scale flow to the circularized structure at smaller radii. These calculations are now in progress, and their results will be reported in the future.

We will first summarize the key physical principles underlying the dynamo process, and then examine what configuration the magnetic field should have in the Keplerian region surrounding Sgr A*. We will then demonstrate that an excellent fit to the sub-mm data is possible with this picture, and discuss the implications of this model to our overall understanding of the environment surrounding the massive black hole at the Galactic Center.

2. The Magnetohydrodynamic Dynamo in a Rotational System

Since the discovery of the local shear instability in weakly magnetized disks (Balbus & Hawley 1991, hereafter BH1), several numerical simulations (Hawley & Balbus 1991, hereafter HB1; Hawley & Balbus 1992, hereafter HB2; Hawley, Gammie & Balbus 1995, hereafter HGB1; Stone, Hawley, Gammie & Balbus 1996, hereafter SHGB) have confirmed the fact that this instability plays a crucial role in rotational accretion systems. A linear analysis (Balbus & Hawley 1992, hereafter BH2) has demonstrated that the instability is extremely powerful. Its maximal growth rate is of the order of the angular velocity, provided that the latter decreases outward and that initially there exists a weak magnetic field. In the case of an axisymmetric perturbation with a weak B_z component of the magnetic field (BH1), the maximal growth rate in a Keplerian disk reaches 0.75Ω at $k_z \simeq \Omega/v_{Az}$, where Ω is the angular velocity, k_z is the z -component of the perturbation wavenumber and $v_{Az} = \sqrt{B_z^2/4\pi\rho}$ is the Alfvén speed in the z -direction. The numerical simulations show that the instability saturates at a turbulent state, producing a significant angular momentum flux, which is dominated by the Maxwell stress rather than the Reynolds stress.

This process has been invoked to account for the origin of the anomalous viscosity in these systems (SHGB).

Another important consequence of this instability, one that we explore at length in this paper, is the amplification of the magnetic field. It has been shown that this instability constitutes a magnetohydrodynamic dynamo (Hawley, Gammie & Balbus 1996, HGB2; Brandenburg, Nordlund & Stein 1995, hereafter BNS). An external magnetic field, which is sometimes invoked to magnetize the disk, is not necessary for the instability to work. An internal turbulent magnetic field can also drive the instability. Once one introduces the complete magnetohydrodynamic equations to describe a shearing hydromagnetic structure, the system saturates at a turbulent state that includes a significant magnetic field energy density. Numerical difficulties with the simulations have thus far prevented the acquisition of quantitative results that may be used directly to describe a real astrophysical situation. However, based on what is now understood about the dynamo process, some very important qualitative results have been obtained, and these can provide a guide to the manner in which the magnetic field grows within the converging flow around a compact object.

2.1. The Basic Equations

For the sake of completeness, let us first analyze how the instability develops in a weakly magnetized Keplerian flow. The basic dynamical equations are (BH1):

$$\frac{d \ln \rho}{dt} + \vec{\nabla} \cdot \mathbf{v} = 0, \quad (1)$$

$$\frac{d\mathbf{v}}{dt} + \vec{\nabla}\Phi = \frac{1}{4\pi\rho}(\mathbf{B} \cdot \vec{\nabla})\mathbf{B} - \frac{1}{\rho}\vec{\nabla} \left(P + \frac{B^2}{8\pi} \right), \quad (2)$$

$$\frac{\partial \mathbf{B}}{\partial t} = (\mathbf{B} \cdot \vec{\nabla})\mathbf{v} - (\vec{\nabla} \cdot \mathbf{v})\mathbf{B} - (\mathbf{v} \cdot \vec{\nabla})\mathbf{B}, \quad (3)$$

where d/dt is the Lagrangian derivative and Φ is the external gravitational potential. The other symbols have their usual meaning. We will adopt standard cylindrical coordinates

(r, ϕ, z) , where r is the perpendicular distance from the z -axis.

Because the maximal growth rate is reached in the axisymmetric case with a weak vertical field, i.e., with $\mathbf{B} = (0, 0, B_z)$, we will here consider perturbations for this specific situation. As such, the Eulerian perturbations, which we denote by δv , δB etc., are modulated by the function $e^{i(k_r r + k_z z - \omega t)}$, where k_r and k_z are, respectively, the radial and vertical components of the wavevector. The numerical simulations show that buoyancy is not a significant factor influencing the instability, nor is the compressibility of the fluid. By neglecting these terms and using the Boussinesq approximation, which consists of setting $\delta \rho = 0$ in all the equations other than the equation of motion and the equation of state, and which also requires that $\delta P = 0$ in the equation of state, one obtains the following linearized dynamical equations:

$$k_r \delta v_r + k_z \delta v_z = 0, \quad (4)$$

$$\frac{\partial \delta v_r}{\partial t} - 2\Omega \delta v_\phi = i \frac{k_z B_z}{4\pi\rho} \delta B_r - i k_r \left(\frac{\delta P}{\rho} + \frac{B_z \delta B_z}{4\pi\rho} \right), \quad (5)$$

$$\frac{\partial \delta v_z}{\partial t} = -i k_z \frac{\delta P}{\rho}, \quad (6)$$

$$\frac{\partial \delta v_\phi}{\partial t} + \frac{\kappa^2}{2\Omega} \delta v_r = i \frac{k_z B_z}{4\pi\rho} \delta B_\phi, \quad (7)$$

$$\frac{\partial \delta B_r}{\partial t} = i k_z B_z \delta v_r, \quad (8)$$

$$\frac{\partial \delta B_z}{\partial t} = i k_z B_z \delta v_z, \quad (9)$$

$$\frac{\partial \delta B_\phi}{\partial t} = \frac{r}{dr} \frac{d\Omega}{dr} \delta B_r + i k_z B_z \delta v_\phi, \quad (10)$$

where Ω is the angular velocity in the circularized flow, and $\kappa^2 = (2\Omega/r) d(r^2\Omega)/dr$ is the square of the epicyclic frequency.

Replacing the Lagrangian derivatives with respect to time t by $-i\omega$ in the linearized equations and eliminating the Eulerian perturbations, one obtains the dispersion relation

$$(\omega^2 - k_z^2 v_{Az}^2)^2 - \frac{k_z^2}{k^2} \kappa^2 (\omega^2 - k_z^2 v_{Az}^2) - 4\Omega^2 \frac{k_z^4 v_{Az}^2}{k^2} = 0, \quad (11)$$

where $k^2 = k_z^2 + k_r^2$. In the case of Keplerian flows, $\kappa = \Omega$. This equation can easily be solved for ω , which yields

$$\omega_0^2 = k_{z0}^2 + \frac{k_{z0}^2}{2 k_0^2} - 2 \sqrt{\frac{k_{z0}^4}{k_0^2} + \frac{k_{z0}^4}{16 k_0^4}}, \quad (12)$$

where $\omega_0 \equiv \omega/\Omega$ and k_0 and k_{z0} are, respectively, k and k_z expressed in units of Ω/v_{Az} . It is noted that ω^2 reaches its minimum value of $-9\Omega^2/16$ when $k^2 = k_z^2 = (15/16)(\Omega/v_{Az})^2$. For $k_r = 0$, the modes become stable when $k_z^2 > 3(\Omega/v_{Az})^2$, and in the long wavelength limit $\omega^2 \simeq -3(v_{Az} k_z)^2$.

In order to appreciate the physical implication of this instability, we examine the fastest growing mode, which occurs when $k^2 = k_z^2 = (15/16)(\Omega/v_{Az})^2$ and $\omega^2 = -9\Omega^2/16$. Solving the linearized equations (4)–(10), we get

$$\delta v_r = \delta v_\phi, \quad (13)$$

$$\delta B_r = -\delta B_\phi, \quad (14)$$

$$\delta B_r = i \frac{4 k_z B_z}{3 \Omega} \delta v_r, \quad (15)$$

$$\delta B_\phi = -i \frac{5}{4} \frac{4\pi\rho\Omega}{k_z B_z} \delta v_\phi, \quad (16)$$

$$\frac{|\delta B_r|^2}{8\pi} = \frac{5}{3} \frac{\rho |\delta v_r|^2}{2}. \quad (17)$$

Keeping the time derivative terms in the linearized equations (4)–(10) and using this solution, we interpret the physics of this unstable mode as follows: The perturbation δv_r , which is generated by δv_ϕ through the Coriolis force term $2\Omega\delta v_\phi$ in Equation (5), induces the perturbation δB_r through Equation (8). Due to the shearing of the disk, the term $r d\Omega/dr \delta B_r$ in Equation (10) then shows that δB_r leads to the production of a perturbation δB_ϕ , which in turn enhances δv_ϕ through the right hand side of Equation (7). Thus a positive feedback loop is established. Some of the other terms in the linearized equations act to stabilize the perturbation, but they are overwhelmed by the positive feedback in the

unstable modes. However, for the modes with a large wavenumber, the term $ik_z B_z \delta v_\phi$ in Equation (10) and the term $ik_z B_z \delta B_r / 4\pi\rho$ in Equation (5) will overwhelm the positive feedback and make the mode stable.

2.2. The Dynamo in Sgr A*

The solution represented by Equation (17) deserves special attention; it says that the turbulent kinetic energy density is approximately equal to the turbulent magnetic field energy density. That is, it points to an equipartition of kinetic and magnetic field energy densities in the final saturated state of the system. Several numerical simulations (BNS, HGB1, HGB2, SHGB) have largely confirmed this result. They show that the ratio of these energy densities in the final turbulent state of the system is only weakly dependent on the initial and subsequent physical conditions assumed in the calculations. We shall therefore here adopt the conclusion drawn from these studies, that in rotational flows

$$\frac{\langle \delta B^2 \rangle}{8\pi} = C_0 \frac{1}{2} \langle \rho \delta v^2 \rangle, \quad (18)$$

where the constant C_0 has a value between 1 and 10, depending on the vertical profile of the Keplerian structure.

Although the above analysis is based on a very specific model, many numerical simulations (BNS, HGB2) have demonstrated that this instability exists more generally, and that even without an external magnetic field, it can produce a significant magnetic energy density, which therefore constitutes a hydromagnetic dynamo. We are here primarily interested in the final saturated state, whose existence has been shown to be inevitable by the numerical simulations. In the following, we will build a simple picture for the dynamo process in Sgr A*, and show how the turbulence is sustained. From these simulations, we infer that the vertical component of the internal turbulent magnetic field can produce

unstable wave modes similar to those produced by an external magnetic field and that the dynamo is driven by them. Since we adopt a zero value for the external magnetic field (a reasonable approximation consistent with the view that the turbulent magnetic field exterior to the Keplerian flow is greatly sub-equipartition, Kowalenko & Melia 1999), the turbulent magnetic field is in fact then the total field \mathbf{B} . Applying the above analysis to the situation in Sgr A*, we replace the external vertical field with the mean-square root ($\sqrt{\langle \delta B_z^2 \rangle} \equiv \sqrt{\langle B_z^2 \rangle}$) of the turbulent magnetic field's vertical component (hereafter the symbol $\langle \rangle$ denotes the mean value of the particular physical quantity). However, because the final state is turbulent, it is expected that the growth rate will be smaller than that in the case where there exists an underlying ordered external field.

Before proceeding with the model, we need to examine whether or not this instability can be damped by Ohmic diffusion for the conditions expected in Sgr A*. Jin (1996) first discussed the possible damping of the shear instability using linear analysis. More recently, this issue was addressed numerically by Fleming, Stone and Hawley (2000). The overall conclusion is that the instability is effectively damped when the diffusion length becomes comparable to the wavelength of the most unstable mode within the latter's growth time scale, i.e., roughly one revolution period. As we have seen, the most unstable wave mode in the Keplerian flow is $k^2 = k_z^2 = 15\Omega/16v_{Az}$, where $v_{Az} = \sqrt{\langle B_z^2 \rangle / 4\pi \langle \rho \rangle}$ is the vertical Alfvén speed of the turbulent magnetic field. As the magnetic field is relatively weak, v_{Az} is small, and all the modes with $k_z < 3\Omega/v_{Az}$ are unstable. These unstable modes lead to an increase in $\langle B_z^2 \rangle$, which in turn leads to an increase in the value of v_{Az} . So the wavelength $\lambda_z = 2\pi/k_z$ of the most unstable mode increases. There does not appear to be any physical reason why the magnetic field should stop increasing before λ_z has reached a value equal to the height H of the Keplerian flow. So the length scale of the most unstable wave mode is expected to be H .

Let us now show that the diffusion length scale within one period in Sgr A* is much smaller than this wavelength. Using the parameter values characterizing the accretion onto this object, we find that the angular velocity of a Keplerian flow near ten Schwarzschild radii ($r_S \equiv 2GM/c^2$, where for Sgr A*, $M \approx 2.6 \times 10^6 M_\odot$) is $\Omega \approx \sqrt{GM/(10r_S)^3} \simeq 0.001 \text{ s}^{-1}$. The temperature of the plasma in this region is expected to be around a few 10^{10} K (Melia 1994; Coker & Melia 2000), so this gas is fully ionized, and its resistivity is (Lyman 1961)

$$\eta = 7.26 \times 10^{-9} \frac{\ln \Lambda}{T^{\frac{3}{2}}} \quad (\text{c.g.s.}) , \quad (19)$$

where the Coulomb logarithm $\ln \Lambda$ is a slowly varying function of the electron density and temperature; 30 is a reasonable value for the conditions at the Galactic Center. Thus, for these parameter values, $\eta \simeq 0.22 \times 10^{-21} \text{ (c.g.s.)}$. The diffusion length scale corresponding to this resistivity is

$$L = \sqrt{\frac{\eta c^2 \tau}{4\pi}} , \quad (20)$$

where τ is the diffusion time, which we set equal to the growth time scale of the most unstable wave mode, i.e., about 1000 s here. Thus, we infer a diffusion length of about 4 cm, which is clearly much smaller than any reasonable value of H , and therefore the characteristic wavelengths of the unstable modes. We conclude that the dynamo in Sgr A* cannot be damped by Ohmic diffusion.

One of the important properties of the final turbulent magnetic field is that it is dominated by its azimuthal component. All the simulations show that the azimuthal component counts for about 80 percent of the total magnetic field energy. This result can be understood by examining the equations describing the evolution of the magnetic energy density (remembering still that the turbulent field generated by the dynamo constitutes the

total field in this system):

$$\frac{1}{2} \frac{\partial B_\phi^2}{\partial t} = r \frac{d\Omega}{dr} B_\phi B_r + B_\phi [\vec{\nabla} \times (\delta \mathbf{v} \times \mathbf{B})]_\phi + \frac{\eta c^2}{4\pi} B_\phi |\nabla^2 \mathbf{B}|_\phi, \quad (21)$$

$$\frac{1}{2} \frac{\partial B_r^2}{\partial t} = B_r [\vec{\nabla} \times (\delta \mathbf{v} \times \mathbf{B})]_r + \frac{\eta c^2}{4\pi} B_r |\nabla^2 \mathbf{B}|_r, \quad (22)$$

$$\frac{1}{2} \frac{\partial B_z^2}{\partial t} = B_z [\vec{\nabla} \times (\delta \mathbf{v} \times \mathbf{B})]_z + \frac{\eta c^2}{4\pi} B_z |\nabla^2 \mathbf{B}|_z, \quad (23)$$

where η is again the resistivity of the plasma, and c is the speed of light. A linear analysis shows that the amplitudes of the azimuthal and radial components of the magnetic field are equal when the perturbation is small, but that the final turbulent state is affected by the nonlinear character of the magnetohydrodynamic equations. As the amplitudes of the perturbation increase, nonlinear effects become more important. Due to the shearing of the Keplerian flow, the average value of $rB_\phi B_r d\Omega/dr$ is positive. The energy Equations (21)—(23) therefore show that $rB_\phi B_r d\Omega/dr$ contributes to a growing anisotropy of the turbulent magnetic field, in the sense that more and more magnetic field energy is generated in the azimuthal direction. For a Keplerian flow with $rd\Omega/dr = -3\Omega/2$, the growth rate due to the shearing of this structure is larger than that associated with any other dynamo process. So the azimuthal component of the magnetic field dominates the final magnetic field energy density.

It is interesting to note that this simple scenario may also be used to interpret the anisotropic spectrum of the turbulent magnetic field energy density observed in the numerical simulations (HGB1). Because the radial magnetic field is stretched in the azimuthal direction, the magnetic energy carried by the modes with the largest wavelengths should be associated mostly with their azimuthal components. However the spectrum for the vertical and radial components should be similar to each other.

So the situation with regard to Sgr A* is the following: as the gas flows inwards and spirals into an approximately Keplerian structure at a distance from the black hole

corresponding to the circularization radius, a linear instability first stretches the magnetic field lines carried by the gas and produces a radial component of \mathbf{B} . The magnetic field generated during this step is approximately in equipartition with the turbulent kinetic energy and counts for a small fraction of its final intensity, but it nonetheless provides the seed for the next step. Second, the shearing in the Keplerian flow stretches the radial magnetic field in the azimuthal direction and it increases the magnetic field energy (as seen, e.g., in HB2). The energy comes from the rotational energy of the gas, and during this process a significant amount of angular momentum can be transported outward as a result of the Maxwell stress $B_r B_\phi / 4\pi$. Finally, some of the magnetic field energy is converted into kinetic energy, which is eventually dissipated into thermal energy as a result of the viscosity, through the Lorentz force term $\mathbf{B} \cdot [\vec{\nabla} \times (\delta \mathbf{v} \times \mathbf{B})]$. In addition, the magnetic field energy may be dissipated through Ohmic resistivity. For example, with their assumed large numerical resistivity, BNS found that about half of the magnetic field energy is dissipated in this way. However, in the case of the Galactic Center, the actual resistivity is rather small and $\eta c^2 / 4\pi r_S \simeq 10^{-13} \text{ cm s}^{-1}$ is insignificant compared to any velocity scale within the plasma. The dissipation of the magnetic field in this fashion is therefore negligible.

So from the magnetic energy Equations (21)–(23), we infer the following proportionality based on dimensional analysis:

$$\frac{\sqrt{\langle \rho \delta v^2 \rangle}}{\sqrt{\langle \rho \rangle} H} \propto r \frac{d\Omega}{dr}, \quad (24)$$

where H is the height of the flow and we have used $\sqrt{\langle \rho \delta v^2 \rangle} / \sqrt{\langle \rho \rangle}$ to characterize the turbulent velocity. Combining Equations (18) and (24), we therefore obtain

$$\sqrt{\langle B^2 \rangle} \propto \sqrt{\langle \rho \rangle} H r \frac{d\Omega}{dr}, \quad (25)$$

which is the main result we have been seeking. Note that for a Keplerian flow, $\Omega = (GM/r^3)^{1/2}$, for which $r d\Omega/dr = -(3/2) \Omega$.

Some support for the validity of this relationship has been provided by the simulations reported in BNS, which include an analysis of the magnetohydrodynamic dynamo at two different radii, one of which is five times smaller than the other. Since this Keplerian flow is characterized by the following equations,

$$(H\Omega)^2 \propto P/\rho, \quad (26)$$

$$\rho \propto r^{15/8}, \quad (27)$$

$$H \propto r^{9/8}, \quad (28)$$

the expression in (25) suggests that $\langle B^2 \rangle \propto P$, the gas pressure. An inspection of the numerical results in BNS shows that the ratio of magnetic field energy density to thermal energy density at the two radii is 0.013 and 0.014. Given that the ratios of the densities, the heights and the angular velocities at the two radii are, respectively, 25, 5, and 10, the constancy of the ratio of magnetic field energy density to thermal energy density is a strong indication that Equation (25) provides an adequate representation of the saturated magnetic field intensity under these conditions. The validity of this expression is also supported by the global simulations of Hawley (2000).

We conclude that the magnetic field intensity within the gas converging onto Sgr A* approaches the functional form given in Equation (25) once the flow settles into a Keplerian structure at small radii. The fluctuations associated with the accreted angular momentum (Coker & Melia 1997) correspond to a circularization radius $\sim 5 - 50 r_S$, so we anticipate that \mathbf{B} will approach the distribution in Equation (25) within this region.

3. Calculation of the Spectrum

3.1. The Anomalous Viscosity

In a Keplerian flow with column density Σ and angular velocity $\Omega = (GM/r^3)^{1/2}$, the radial velocity v_r at (cylindrical) radius r is given as (e.g., Stoeger 1980)

$$v_r = -\frac{3}{r^{1/2}\Sigma} \frac{\partial}{\partial r} (\nu \Sigma r^{1/2}) , \quad (26)$$

where ν is the kinematic viscosity,

$$\nu = \frac{2}{3} \frac{W_{r\phi}}{\Sigma \Omega} , \quad (27)$$

and $W_{r\phi}$ is the vertically integrated sum of the Maxwell and Reynolds stresses (Balbus et al. 1994). For the problem at hand, the Maxwell stress dominates, and

$$W_{r\phi} \approx \beta_\nu \int dz \left\langle \frac{B^2}{8\pi} \right\rangle \quad (28)$$

(the average inside the integral being taken over time). Even though this approximation is valid simply on the basis that the Reynolds stress is relatively small, its validity is enhanced by the fact that since the turbulent velocity (which accounts for this kinetic stress) and \mathbf{B} are generated by the same process, both should be scalable by \mathbf{B} . Numerical simulations (e.g., by Brandenburg, et al. 1995) show that β_ν changes very slowly with r . In the particular cases considered by these authors, β_ν ranged in value from ≈ 0.1 to 0.2 , which represents an increase by a factor of only 2 as r decreased by a factor of 5. For simplicity, we will here adopt a “mean” value of ~ 0.15 for this quantity.

To use the result of § 2.2, we first need to know the vertical structure of the Keplerian flow. For steady conditions, one can obtain the vertical profile by assuming that the gas is (on average) in local hydrostatic equilibrium. Balancing gravity and the pressure gradient in the vertical direction, we obtain the scale height

$$H = \sqrt{\frac{2R_g T r^3}{\mu GM}} , \quad (29)$$

where T is the gas temperature at radius r , R_g is the gas constant, and μ is the molecular weight. As an approximation, we will assume that the Keplerian flow is axisymmetric and is independent of the vertical coordinate. Written another way, we have

$$(H\Omega)^2 = 2P/\rho . \quad (30)$$

Following the result of § 2.2, we will write

$$\int dz \langle \frac{B^2}{8\pi} \rangle \approx \beta_p \int P dz = \beta_p \frac{R_g \Sigma T}{\mu} , \quad (31)$$

where β_p is roughly constant with a value of ≈ 0.02 . Thus, with

$$\dot{M} = -2\pi r \Sigma v_r , \quad (32)$$

we can integrate Equation (26) to obtain

$$v_r = \frac{rT(r)}{T_0 r_0 / v_{r0} + \mu (GM)^{1/2} (r_0^{1/2} - r^{1/2}) / \beta_\nu \beta_p R_g} , \quad (33)$$

where the quantities with subscript 0 are to be evaluated at the outer edge of the Keplerian flow (i.e., at radius r_0).

3.2. Energy Equations for the Keplerian Flow

In order to get the radial dependence of the flow, we need to solve the energy equation to determine the temperature. The gas is heated primarily by Ohmic diffusion (which converts magnetic field energy to thermal energy) and viscous dissipation, and is cooled by synchrotron and bremsstrahlung emission. Equation (1) is always valid. By incorporating Ohmic diffusion and viscous dissipation, Equations (2) and (3) take the form:

$$\frac{d(\rho \mathbf{v})}{dt} + \rho \vec{\nabla} \Phi + \rho \mathbf{v} (\vec{\nabla} \cdot \mathbf{v}) = \frac{1}{4\pi} (\mathbf{B} \cdot \vec{\nabla}) \mathbf{B} - \vec{\nabla} \left(P_{th} + \frac{B^2}{8\pi} \right) + 2 \vec{\nabla} \cdot (\mathbf{S} \rho \nu) , \quad (34)$$

$$\frac{\partial \mathbf{B}}{\partial t} = \vec{\nabla} \times (\mathbf{v} \times \mathbf{B}) - \frac{c^2 \eta}{4\pi} \vec{\nabla} \times (\vec{\nabla} \times \mathbf{B}) , \quad (35)$$

respectively, where $S_{ij} = (1/2)[v_{i,j} + v_{j,i} - (2/3)\delta_{ij}v_{k,k}]$ and $P_{th} = \rho R_g T / \mu + P_{rad}$ is the non-magnetic pressure. For a Keplerian flow, $S_{r\phi} = -(3/4)\Omega$. The radiation pressure, P_{rad} , is given in the Rayleigh-Jeans approximation:

$$P_{rad} = \frac{8\pi}{9} kT \left(\frac{\nu_m}{c} \right)^3, \quad (36)$$

where ν_m is the frequency below which the radiative emission is highly absorbed, so that the optical depth from r to infinity is unity (see Melia 1994).

Projecting Equation (34) onto the vector \mathbf{v} and Equation (35) onto the vector \mathbf{B} , we eventually find that

$$\begin{aligned} \frac{\partial}{\partial t} \left[\rho \left(\frac{1}{2} v^2 + \Phi \right) \right] &= -\vec{\nabla} \cdot \left[\rho \mathbf{v} \left(\frac{1}{2} v^2 + \Phi \right) \right] - \mathbf{v} \cdot \vec{\nabla} P_{th} + 2\mathbf{v} \cdot \vec{\nabla} \cdot (\mathbf{S} \rho \nu) \\ &\quad - \frac{1}{4\pi} \mathbf{v} \cdot [\mathbf{B} \times (\vec{\nabla} \times \mathbf{B})], \end{aligned} \quad (37)$$

$$\frac{\partial}{\partial t} \left(\frac{B^2}{8\pi} \right) = \frac{1}{4\pi} \mathbf{B} \cdot [\vec{\nabla} \times (\mathbf{v} \times \mathbf{B})] + \frac{c^2 \eta}{16\pi^2} \vec{\nabla} \cdot [\mathbf{B} \times (\vec{\nabla} \times \mathbf{B})] - \eta \mathbf{J}^2, \quad (38)$$

where $\mathbf{J} = (c/4\pi) \vec{\nabla} \times \mathbf{B}$ is the current density. Adding the two equations gives

$$\begin{aligned} \frac{\partial}{\partial t} \left[\frac{B^2}{8\pi} + \rho \left(\frac{1}{2} v^2 + \Phi \right) \right] &= -\vec{\nabla} \cdot \left[-2\nu \rho \mathbf{v} \cdot \mathbf{S} + \frac{1}{4\pi} \mathbf{B} \times \left(\mathbf{v} \times \mathbf{B} - \frac{c^2 \eta}{4\pi} \vec{\nabla} \times \mathbf{B} \right) \right. \\ &\quad \left. + \rho \mathbf{v} \left(\frac{1}{2} v^2 + \Phi \right) \right] - \eta \mathbf{J}^2 - 2\nu \rho \mathbf{S}^2 - \mathbf{v} \cdot \vec{\nabla} P_{th}. \end{aligned} \quad (39)$$

In steady state, the heating term is therefore inferred to be

$$\begin{aligned} \Gamma &\equiv \eta \mathbf{J}^2 + 2\nu \rho \mathbf{S}^2 \\ &= -\vec{\nabla} \cdot \left[\rho \mathbf{v} \left(\frac{1}{2} v^2 + \Phi \right) + \frac{1}{4\pi} \mathbf{B} \times (\mathbf{v} \times \mathbf{B} - \frac{c^2 \eta}{4\pi} \vec{\nabla} \times \mathbf{B}) - 2\nu \rho \mathbf{v} \cdot \mathbf{S} \right] - \mathbf{v} \cdot \vec{\nabla} P_{th} \end{aligned} \quad (40)$$

Following the argument by Balbus (1994), we see that the divergence of the viscous flux and Ohmic flux is insignificant, and so we can neglect these terms in the following discussion.

In a Keplerian flow, the velocity fluctuations are small compared to the azimuthal component of the velocity and it is the correlated fluctuations in the velocity and

magnetic field components that produces the anomalous viscosity (Balbus et al. 1994). So $\mathbf{v} = v_\phi \mathbf{e}_\phi + \delta \mathbf{v}$, with δv much smaller than $v_\phi \equiv \sqrt{GM/r}$. Introducing this into Equation (40) and neglecting the high order terms, we get the steady state heating rate

$$\begin{aligned} \Gamma = & -\mathbf{v} \cdot \vec{\nabla} P_{th} - \frac{1}{Hr} \frac{\partial}{\partial r} \left(\frac{v_r Hr < B^2 >}{4\pi} \right) \\ & - \frac{1}{Hr} \frac{\partial}{\partial r} \left[Hr \rho v_r \left(\frac{1}{2} v_\phi^2 + \frac{1}{2} v_r^2 + \Phi \right) + Hr v_\phi \left\langle \rho v_r \delta v_\phi - \frac{B_r B_\phi}{4\pi} \right\rangle \right], \end{aligned} \quad (41)$$

where the correlated fluctuation on the right hand side is given by

$$\left\langle \rho v_r \delta v_\phi - \frac{B_r B_\phi}{4\pi} \right\rangle = \frac{W_{r\phi}}{2H}. \quad (42)$$

Next, the temperature can be determined by solving the thermal energy conservation equation:

$$\frac{\partial(\rho\epsilon)}{\partial t} = -\vec{\nabla} \cdot (\mathbf{v}\rho\epsilon) + \Gamma - \Lambda - P_{th} \vec{\nabla} \cdot \mathbf{v}, \quad (43)$$

where Λ is the cooling rate, and $\rho\epsilon = \alpha nkT + 3P_{rad}$ is the thermal and radiation energy density. In the fully ionized but non-relativistic limit, $\alpha = 3$, whereas in the relativistic electron limit, $\alpha = 9/2$. Adding Equations (39) and (43), we have the complete energy conservation equation of the system

$$\begin{aligned} \frac{\partial}{\partial t} \left[\frac{B^2}{8\pi} + \rho \left(\frac{1}{2} v^2 + \Phi + \epsilon \right) \right] = & -\eta \mathbf{J}^2 - 2\nu \rho \mathbf{S}^2 - \Lambda - \vec{\nabla} \cdot \left[\rho \mathbf{v} \left(\frac{P_{th}}{\rho} + \frac{1}{2} v^2 + \Phi + \epsilon \right) \right. \\ & \left. - 2\nu \rho \mathbf{v} \cdot \mathbf{S} + \frac{1}{4\pi} \mathbf{B} \times (\mathbf{v} \times \mathbf{B} - \frac{c^2 \eta}{4\pi} \vec{\nabla} \times \mathbf{B}) \right] + \Gamma. \end{aligned} \quad (44)$$

In steady state, the derivative with respect to time equals zero. So using the mass conservation Equation (32) for a Keplerian flow and Equations (41), (42), (28) and (31),

we have

$$\begin{aligned}
\rho v_r \frac{\partial \epsilon}{\partial r} &= \Gamma - \Lambda - P_{th} \vec{\nabla} \cdot \mathbf{v} \\
&= -\Lambda - \vec{\nabla} \cdot (\mathbf{v} P_{th}) + \frac{1}{Hr} \frac{\partial}{\partial r} \left(\frac{\beta_p R_g T \dot{M}}{2\pi\mu} \right) \\
&\quad + \frac{1}{Hr} \frac{\partial}{\partial r} \left[\frac{\dot{M}}{4\pi} \left(\frac{1}{2}(v_\phi^2 + v_r^2) + \Phi \right) + \frac{\dot{M} \beta_\nu \beta_p R_g T v_\phi}{4\pi v_r \mu} \right].
\end{aligned} \tag{45}$$

The temperature equation follows from this once we substitute for H , ϵ , P_{th} etc., whence

$$C_1 \frac{T'}{T} = -\frac{\Lambda}{\rho v_r} + C_2, \tag{46}$$

where

$$\begin{aligned}
C_1 &= \epsilon + \frac{P_{th}}{\rho} - \frac{1}{2}v_r^2 + \frac{2\beta_p R_g T}{\mu} + \frac{3\beta_\nu \beta_p R_g T v_\phi}{2\mu v_r}, \\
C_2 &= \frac{5}{2r}v_r^2 - \frac{GM}{2r^2} + \frac{\rho'}{\rho} \left[\frac{32\pi R_g T}{9n} \left(\frac{\nu_m}{c} \right)^3 + v_r^2 - \frac{\beta_\nu \beta_p R_g T v_\phi}{\mu v_r} \right] \\
&\quad - \frac{32\pi R_g T}{3n} \left(\frac{\nu_m}{c} \right)^3 \frac{\nu'_m}{\nu_m} - \frac{\beta_\nu \beta_p R_g T v_\phi}{\mu v_r} \frac{2}{r}.
\end{aligned} \tag{47}$$

The 's denote derivatives with respect to r .

Now, from Equations (29), (32) and (33), we find that

$$\frac{T'}{2T} + \frac{3}{2r} = \frac{H'}{H}, \tag{48}$$

$$\frac{1}{r} + \frac{v'_r}{v_r} + \frac{H'}{H} + \frac{\rho'}{\rho} = 0, \tag{49}$$

$$\frac{T'}{T} + \frac{1}{r} + \frac{\mu \sqrt{GM} v_r}{2\beta_\nu \beta_p R_g r \sqrt{r} T} = \frac{v'_r}{v_r}. \tag{50}$$

Thus,

$$\frac{\rho'}{\rho} = -\frac{7}{2r} - \frac{3T'}{2T} - \frac{\mu \sqrt{GM} v_r}{2\beta_\nu \beta_p R_g r \sqrt{r} T}. \tag{51}$$

Therefore eliminating ρ' in Equation (46), we get a differential equation for the temperature:

$$E_1 T' = E_2 - \frac{\Lambda}{\rho v_r R_g} - \frac{32\pi T}{3n} \left(\frac{\nu_m}{c} \right)^3 \frac{\nu'_m}{\nu_m}, \tag{52}$$

where

$$\begin{aligned}
E_1 &= \alpha + 2 + \frac{32\pi}{9n} \left(\frac{\nu_m}{c} \right)^3 + \frac{2\beta_p}{\mu} + \frac{3\beta_\nu\beta_p v_\phi}{2\mu v_r} - \frac{v_r^2}{2R_g T} + \frac{3}{2}E_3, \\
E_2 &= -\frac{2T}{r} \frac{\beta_\nu\beta_p v_\phi}{\mu v_r} + \left(\frac{5}{2r} v_r^2 - \frac{GM}{2r^2} \right) \frac{1}{R_g} - E_3 T \left(\frac{7}{2r} + \frac{\mu\sqrt{GM}v_r}{2\beta_\nu\beta_p R_g r \sqrt{r} T} \right), \\
E_3 &= \frac{v_r^2}{R_g T} - \frac{\beta_\nu\beta_p v_\phi}{\mu v_r} + \frac{32\pi}{9n} \left(\frac{\nu_m}{c} \right)^3.
\end{aligned} \tag{53}$$

Using the characteristic parameters for Sgr A*, we find that the radiation energy density and pressure are always negligible compared to those for the gas within the Keplerian flow. So, in Equation (52) we will neglect those terms that depend on ν_m . Thus this equation provides the temperature profile throughout the inner region once the outer boundary conditions are specified.

3.3. Calculation of the Spectrum

The flux density (at earth) produced by the Keplerian portion of the flow is given by

$$F_{\nu_0} = \frac{1}{D^2} \int I_{\nu'} \sqrt{1 - r_S/r} \, dA, \tag{54}$$

where $D = 8.5$ kpc is the distance to the Galactic Center, ν_0 is the observed frequency at infinity and ν' is the frequency measured by a stationary observer in the Schwarzschild frame. (For simplicity, we here assume the metric for a non-spinning black hole. A more thorough exploration of the parameter values, including the black hole spin, will be discussed elsewhere.) The frequency transformations are given by

$$\nu_0 = \nu' \sqrt{1 - r_S/r}, \tag{55}$$

$$\nu' = \nu \frac{\sqrt{1 - v_\phi^2/c^2}}{1 - (v_\phi/c) \cos \theta}, \tag{56}$$

where ν is the frequency measured in the co-moving frame, and θ is the angle between the velocity \vec{v}_ϕ and the line of sight. Since the radial velocity is always much smaller than v_ϕ , we ignore this component in the transformation equations. So $\cos \theta = \sin i \cos \phi$, where i is the inclination angle of the axis perpendicular to the Keplerian flow, and ϕ is the azimuth of the emitting element. When the Doppler shift is included, the blue shifted region is located primarily near $\phi = 0$ while the red shifted region is at $\phi = \pi$. The other quantities that are necessary for an evaluation of the flux density are the area element

$$dA = \frac{1}{\sqrt{1 - r_S/r}} \cos i \, r \, dr \, d\phi , \quad (57)$$

and the specific intensity

$$I_{\nu'} = B_{\nu'}(1 - e^{-\tau}) , \quad (58)$$

where

$$B_{\nu'} = \left(\frac{\sqrt{1 - v_\phi^2/c^2}}{1 - (v_\phi/c) \cos \theta} \right)^3 B_\nu , \quad (59)$$

and the optical depth is

$$\tau = \int \kappa'_{\nu'} \, ds = \kappa_\nu \frac{2H}{\cos i} \frac{1 - (v_\phi/c) \cos \theta}{\sqrt{1 - v_\phi^2/c^2}} , \quad (60)$$

where κ_ν is the absorption coefficient. In the case where the optical depth $\tau \ll 1$, Kirchoff's law allows us to write

$$I_{\nu'} \approx B_{\nu'} \tau = \epsilon_\nu \frac{2H}{\cos i} \left(\frac{\sqrt{1 - v_\phi^2/c^2}}{1 - (v_\phi/c) \cos \theta} \right)^2 , \quad (61)$$

where $\epsilon_\nu = B_\nu \kappa_\nu$ is the emissivity. The presence of a substantial azimuthal component of the magnetic field makes it convenient to calculate the observed flux directly from the Extraordinary and Ordinary components of the intensity. The most convenient approach is

to select the symmetry axis of the Keplerian flow as the reference direction. The observed flux densities in the azimuthal and the reference directions are given by

$$F_{1\nu_0} = \frac{1}{D^2} \int (I_{\nu'}^e |\cos \phi'| + I_{\nu'}^o |\sin \phi'|) \sqrt{1 - r_S/r} \, dA , \quad (62)$$

$$F_{2\nu_0} = \frac{1}{D^2} \int (I_{\nu'}^e |\sin \phi'| + I_{\nu'}^o |\cos \phi'|) \sqrt{1 - r_S/r} \, dA , \quad (63)$$

respectively, where $\phi' + \pi/2$ is the position angle of the magnetic field vector within the emitting element that has an azimuth of ϕ , so that $\cot \phi' = \cot \phi \cos i$. $I_{\nu'}^e$ and $I_{\nu'}^o$ are the specific intensities for the Extraordinary and Ordinary waves, respectively. For thermal synchrotron radiation, the emissivities are given by (Pacholczyk 1970)

$$\epsilon^e = \frac{\sqrt{3}e^3}{8\pi m_e c^2} B \sin \theta' \int_0^\infty N(E)[F(x) + G(x)] \, dE , \quad (64)$$

$$\epsilon^o = \frac{\sqrt{3}e^3}{8\pi m_e c^2} B \sin \theta' \int_0^\infty N(E)[F(x) - G(x)] \, dE , \quad (65)$$

where $N(E)$ is the electron distribution function at energy E , and

$$\cos \theta' = \frac{\cos \theta - v_\phi/c}{1 - (v_\phi/c) \cos \theta} , \quad (66)$$

$$x = \frac{4\pi\nu m_e^3 c^5}{3eB \sin \theta' E^2} , \quad (67)$$

$$F(x) = x \int_x^\infty K_{5/3}(z) \, dz , \quad (68)$$

$$G(x) = x K_{2/3}(x) . \quad (69)$$

$K_{5/3}$ and $K_{2/3}$ are the corresponding modified Bessel functions. The total flux density produced by the Keplerian portion of the flow is the sum of these two.

3.4. Results

Not all the solutions to Equation (52) are physically acceptable. Equation (33) shows that for given parameters β_p and β_ν , some boundary values of T_0 , r_0 and v_{r0} will make the

denominator vanish at a critical radius r_{crit} . For a physically meaningful flow, we therefore need $r_{crit} \leq r_i$, where r_i is the inner boundary of the Keplerian flow ($r_i = r_S$ in the following discussion). For simplicity, we shall set $r_{crit} = r_i$, for which

$$\frac{T_0 r_0}{v_{r0}} + \frac{\mu(GM)^{1/2}(r_0^{1/2} - r_i^{1/2})}{\beta_\nu \beta_p R_g} = 0 . \quad (70)$$

This fixes T_0 in terms of r_0 and v_{r0} .

A second constraint is provided directly by the current IR and UV observations of Sgr A*, which rule out the possible presence of an optically thick disk. Working within these constraints, the best fit model for the sub-millimeter bump is that shown in Figures 1-7. The latest Chandra observation (indicating a luminosity for Sgr A* of no more than 2.73×10^{33} ergs s⁻¹ between 2 and 10 keV) restricts the possible range of \dot{M} near the black hole. The reason for this can be understood qualitatively as follows.

The requirement that the flow remains optically thin in the Keplerian region (i.e., within the nominal 5 r_S we are considering here) means that $n\sigma_T H \leq \cos i$, where $\sigma_T = 6.65 \times 10^{-25}$ cm² is the Thomson scattering cross section. By using Equation (32) and $\Sigma = 2Hnm_p$, we therefore have

$$\dot{M} \leq -4\pi m_p r v_r \cos i / \sigma_T . \quad (71)$$

But Equations (70) and (33) show that

$$-v_r = \frac{Tr\beta_\nu\beta_p R_g}{\mu(GM)^{1/2}(r^{1/2} - r_i^{1/2})} . \quad (72)$$

Combining these two relations, we get

$$\dot{M} \leq 5.7 \times 10^{19} \frac{\cos i}{\sqrt{r/r_i} - 1} \left(\frac{r}{r_i}\right)^2 \left(\frac{T}{10^{11} \text{ K}}\right) \left(\frac{\beta_\nu}{0.15}\right) \left(\frac{\beta_p}{0.02}\right) \text{ g s}^{-1} . \quad (73)$$

Since the factor $(r/r_i)^2/(\sqrt{r/r_i} - 1)$ has a minimum value of $4^4/3^3$ at $r = 16/9 r_S$, and the Keplerian flow must be optically thin everywhere

$$\dot{M} \leq 5.4 \times 10^{20} \cos i \left(\frac{T_m}{10^{11} \text{ K}}\right) \left(\frac{\beta_\nu}{0.15}\right) \left(\frac{\beta_p}{0.02}\right) \text{ g s}^{-1} . \quad (74)$$

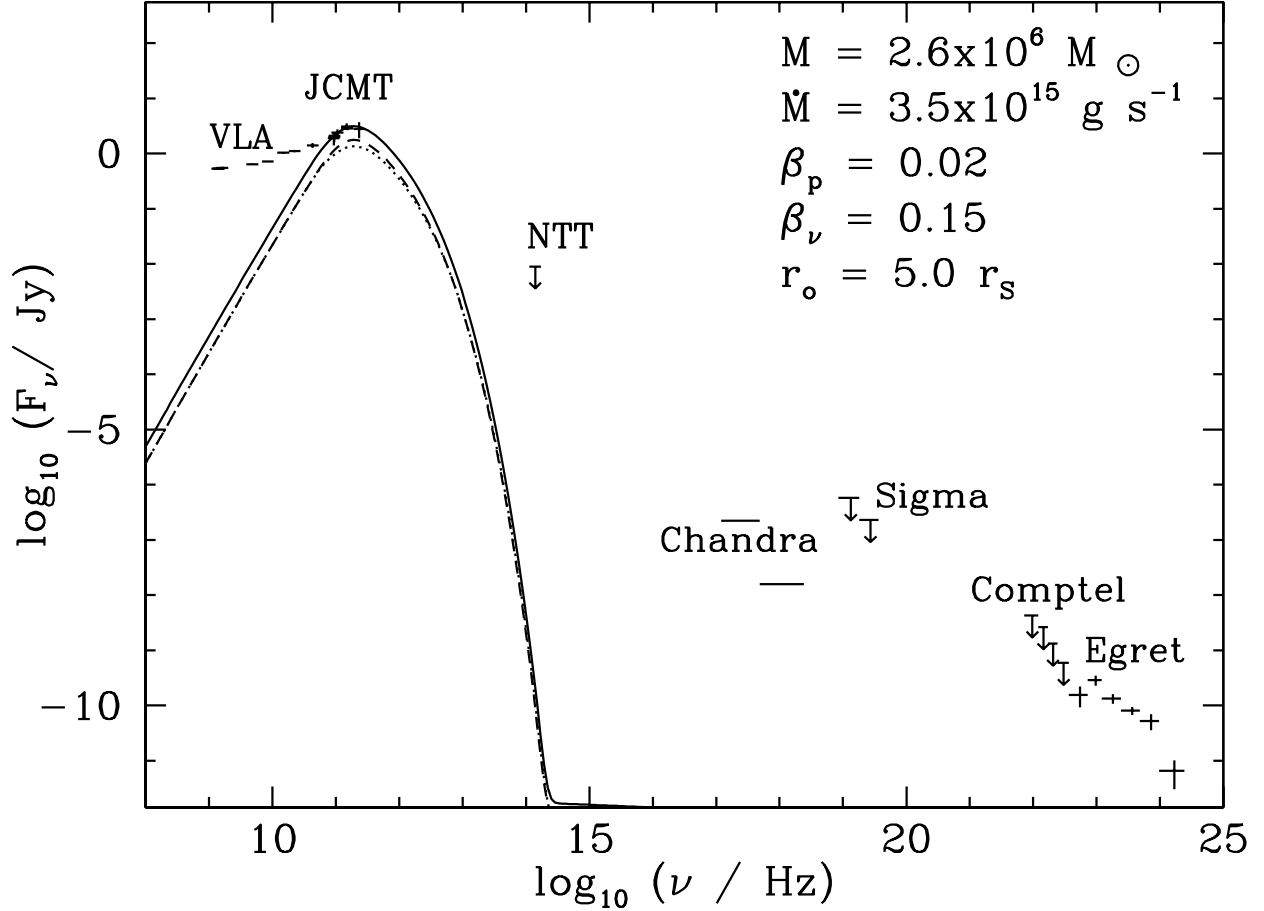


Fig. 1.— The spectrum corresponding to the best fit model, whose parameter values are indicated within the figure itself. The dashed curve corresponds to the second component. The dotted curve corresponds to the first component. The solid curve is the sum of these two. The disk has an inclination angle of 60° . It is also necessary to specify the ratio of v_r to its free-fall value at r_0 . For this model, this ratio is 4.0×10^{-4} . The references for the data are given in the text.

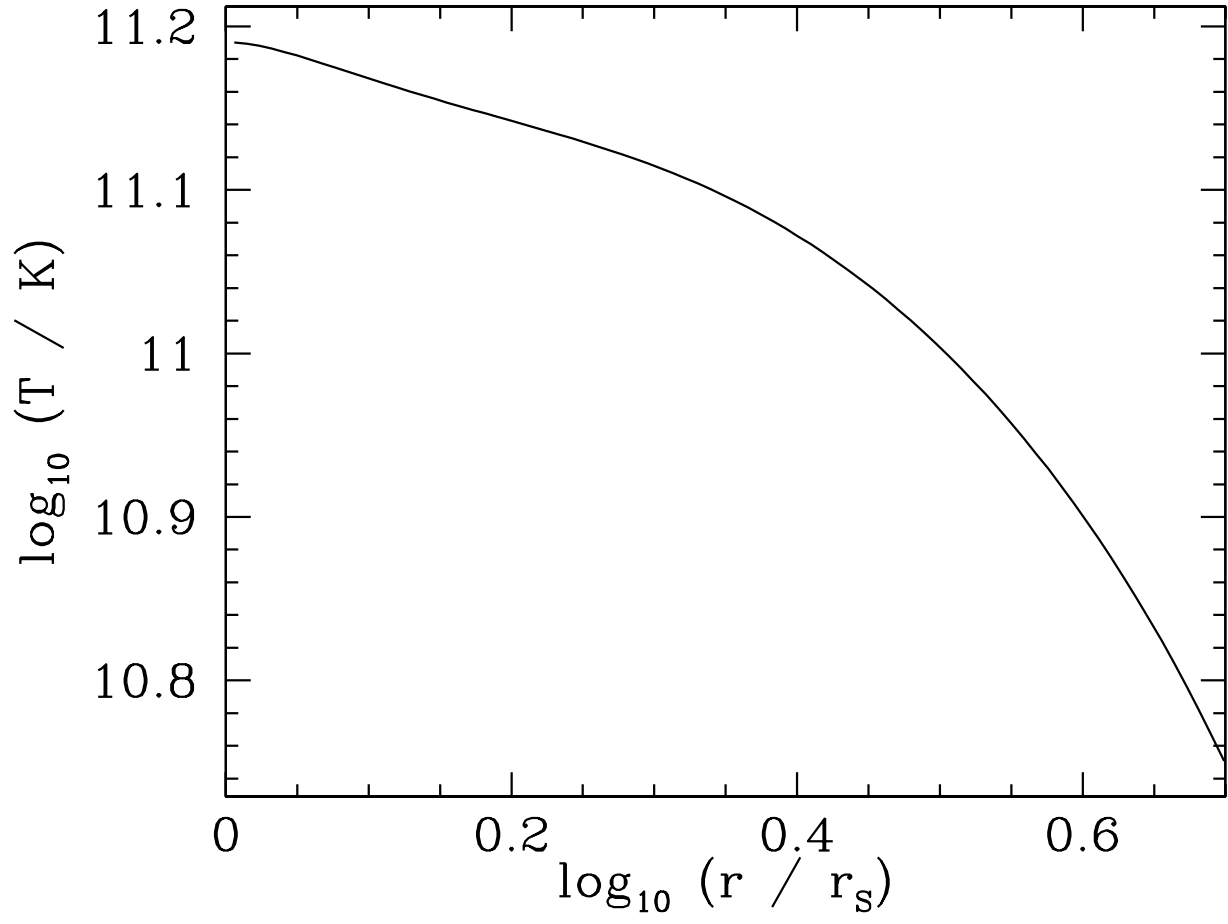


Fig. 2.— Temperature profile corresponding to the best fit model, shown in Figure 1.

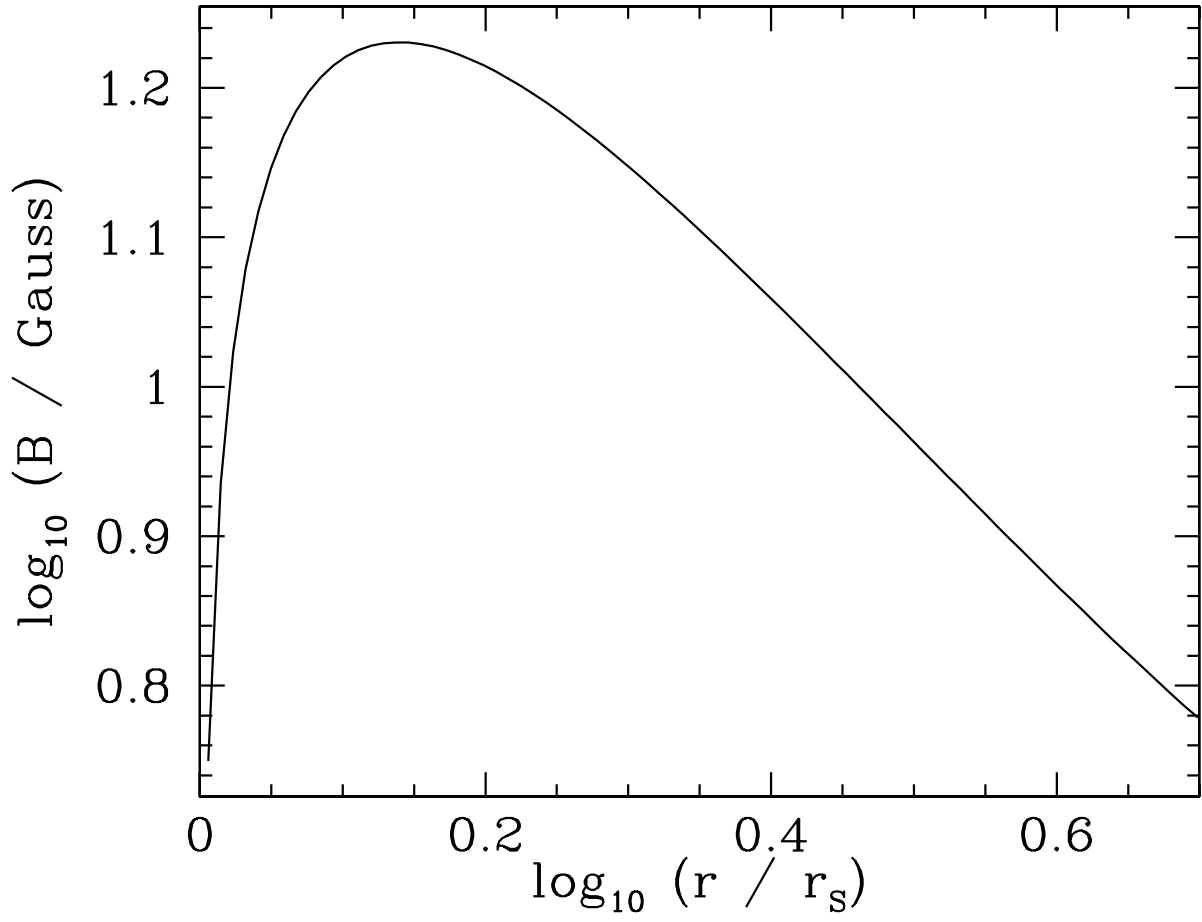


Fig. 3.— Magnetic field intensity corresponding to the best fit model, shown in Figure 1.

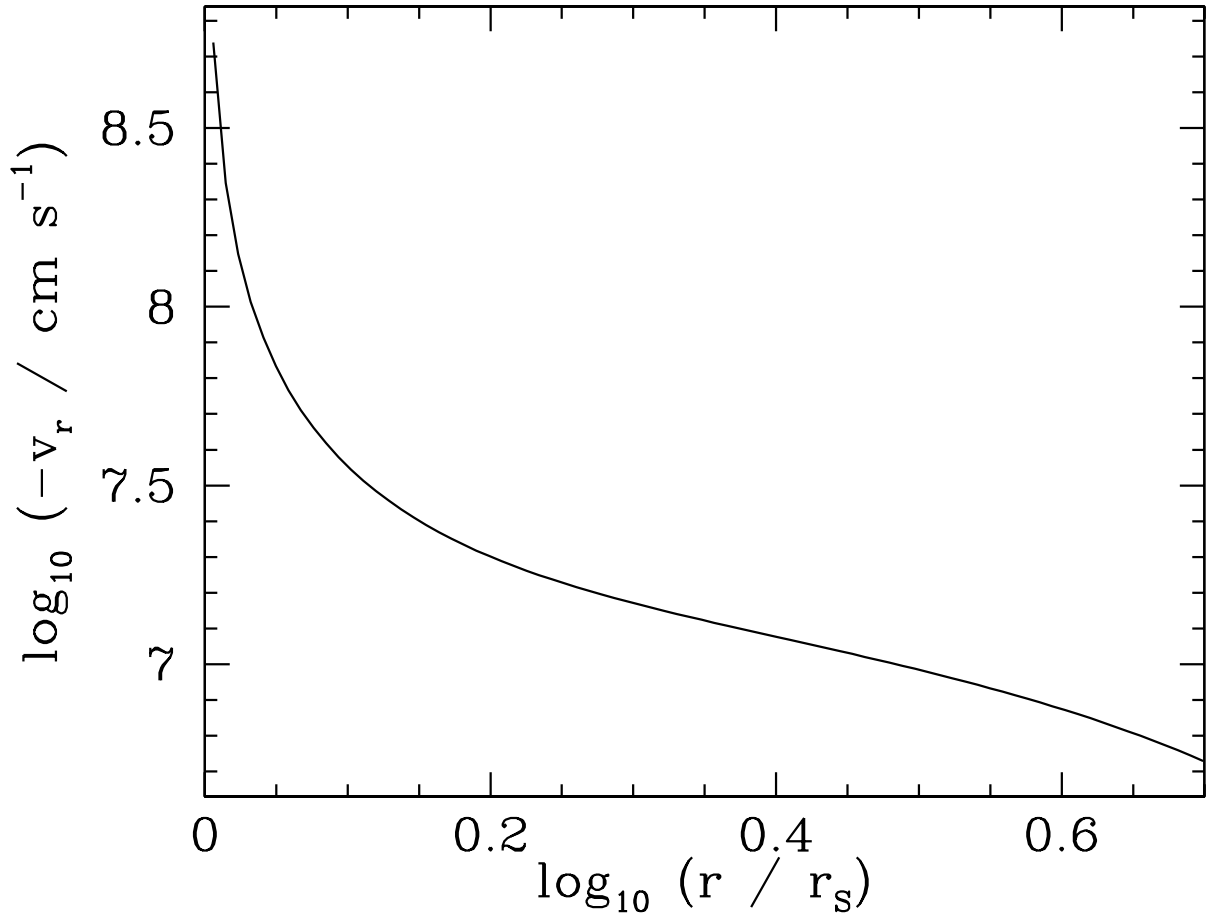


Fig. 4.— Radial velocity profile corresponding to the best fit model, shown in Figure 1.

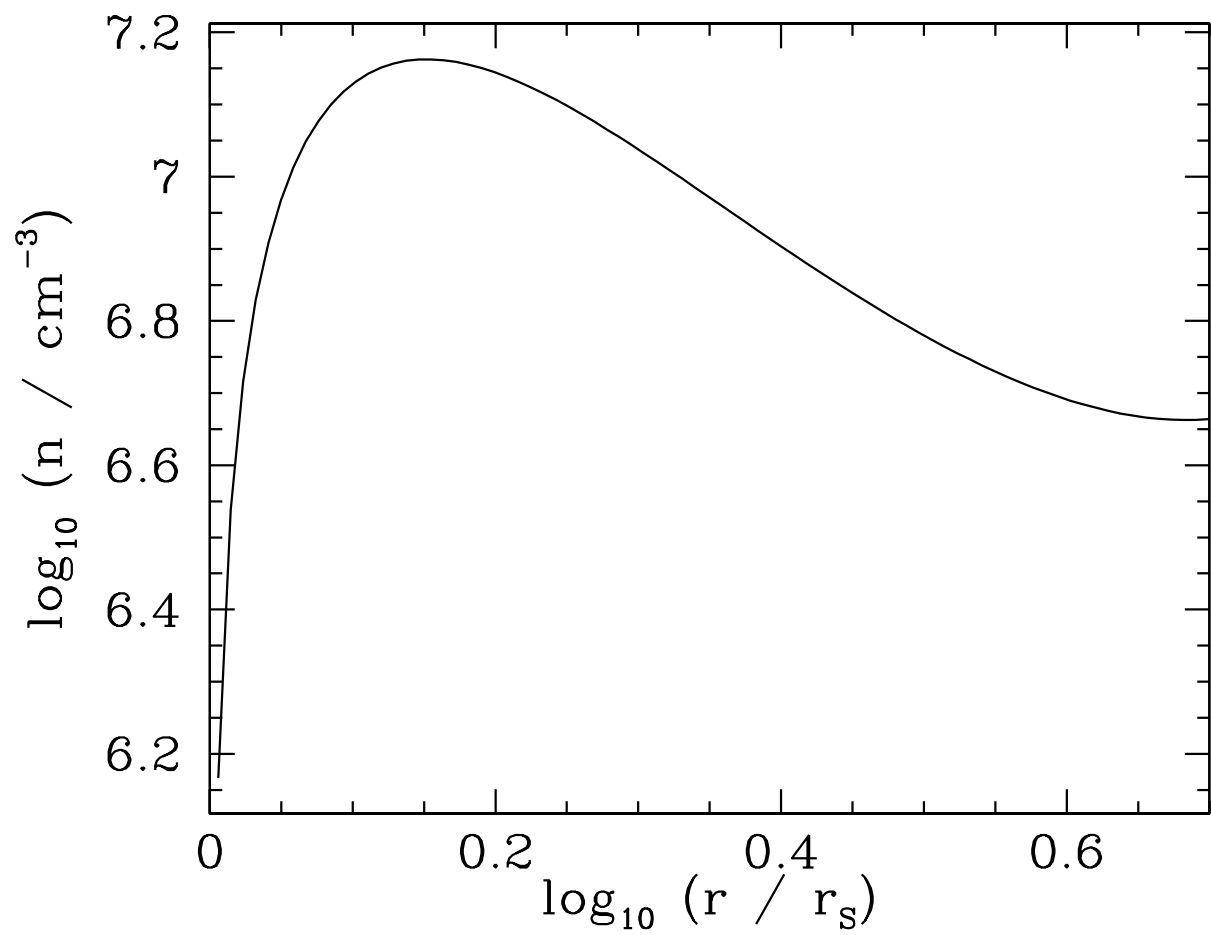


Fig. 5.— Particle number density corresponding to the best fit model, shown in Figure 1.

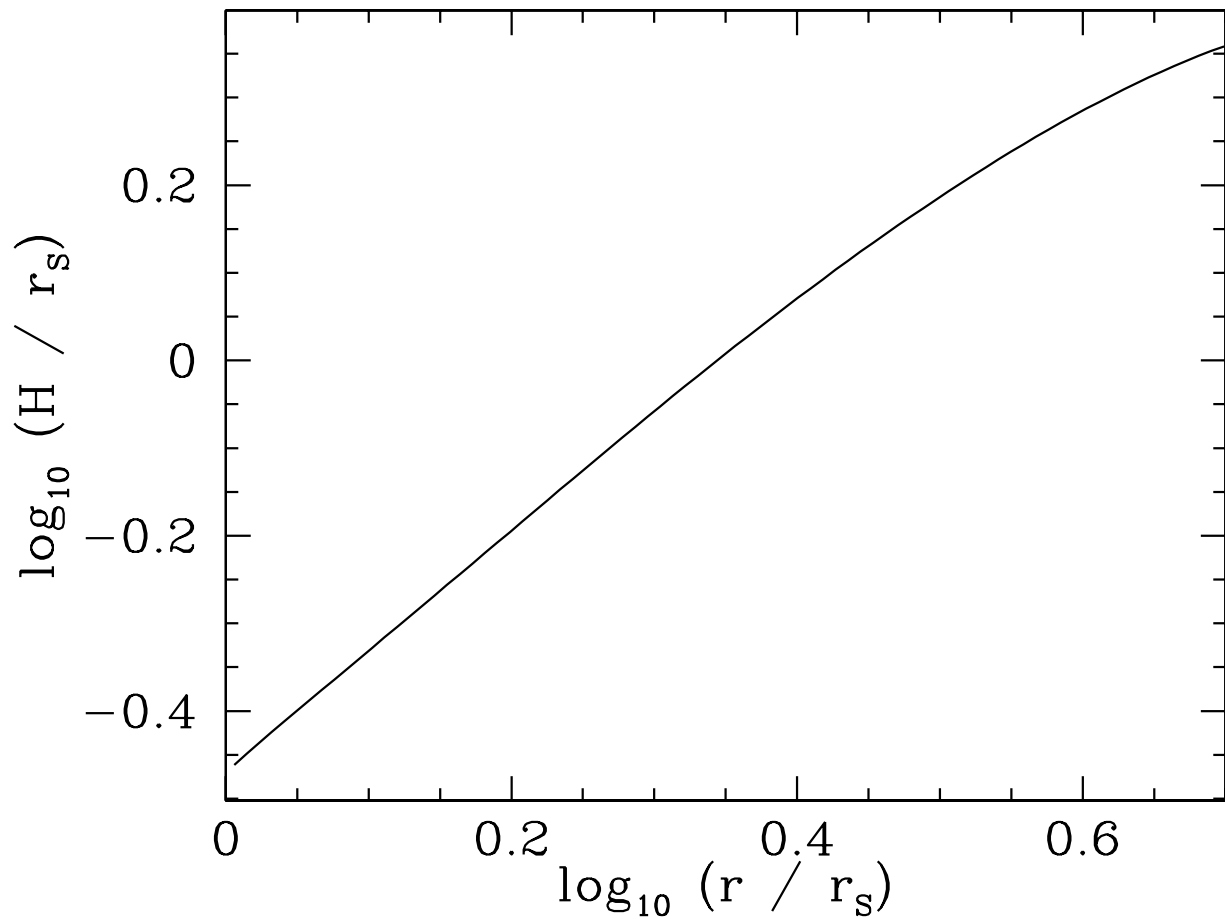


Fig. 6.— Scale height of the gas as a function of r , divided by the Schwarzschild radius, for the best fit model, shown in Figure 1.

where T_m is the maximal temperature. In itself, this value is consistent with the Bondi-Hoyle rate inferred from the simulations by Coker & Melia (1997).

An even stricter upper limit for the accretion rate can be obtained if we assume that the sub-millimeter bump in the radio is produced by a hot Keplerian flow through synchrotron emission. This plasma will also produce X-radiation via bremsstrahlung emission. The bremsstrahlung emissivity is given by

$$\epsilon_b = 6.8 \times 10^{-38} n^2 T^{-0.5} e^{-h\nu/kT} \text{ ergs cm}^{-3} \text{ s}^{-1} \text{ Hz}^{-1}. \quad (75)$$

In the Keplerian flow, $h\nu \ll kT$ within the 2 – 10 keV energy range. Thus, with $\exp(-h\nu/kT) \approx 1$, we have

$$L = \int_{2 \text{ keV}}^{10 \text{ keV}} \frac{d(h\nu)}{h} \int_{r_i}^{r_0} dr 4\pi r H \epsilon_b = 2.73 \times 10^{33} \text{ ergs s}^{-1}, \quad (76)$$

and using Equation (32), this gives

$$\dot{M}^2 \int_{r_i}^{r_0} \frac{dr}{v_r^2 H r \sqrt{T}} \leq 0.71 \times 10^6 \quad (77)$$

in c.g.s. units. But from Equations (72) and (29) we have (again in c.g.s. units)

$$\begin{aligned} \int_{r_i}^{r_0} \frac{dr}{v_r^2 H r \sqrt{T}} &\geq 8.7 \times 10^{-29} \int_1^{r_0/r_i} \left(\frac{10^{11} \text{ K}}{T} \right)^3 \left(\frac{0.15}{\beta_\nu} \right)^2 \left(\frac{0.02}{\beta_p} \right)^2 \frac{(\sqrt{x} - 1)^2}{x^{4.5}} dx \\ &\geq 1.74 \times 10^{-28} \left(\frac{10^{11} \text{ K}}{T_m} \right)^3 \left(\frac{0.15}{\beta_\nu} \right)^2 \left(\frac{0.02}{\beta_p} \right)^2 \left(\frac{1}{105} - \frac{1}{5x_0^{2.5}} + \frac{1}{3x_0^3} - \frac{1}{7x_0^{3.5}} \right), \end{aligned} \quad (78)$$

where $x_0 = r_0/r_i$. So

$$\dot{M} \leq 6.4 \times 10^{16} \left(\frac{T_m}{10^{11} \text{ K}} \right)^{1.5} \left(\frac{\beta_\nu}{0.15} \right) \left(\frac{\beta_p}{0.02} \right) \left(\frac{1}{105} - \frac{1}{5x_0^{2.5}} + \frac{1}{3x_0^3} - \frac{1}{7x_0^{3.5}} \right)^{-0.5} \text{ g s}^{-1}. \quad (79)$$

We point out here that the range of values giving reasonable fits to the sub-mm data (e.g., Fig. 1) falls below this limit, though close to it. Thus, the current high-energy observations of Sgr A* do not appear to be in conflict with this model.

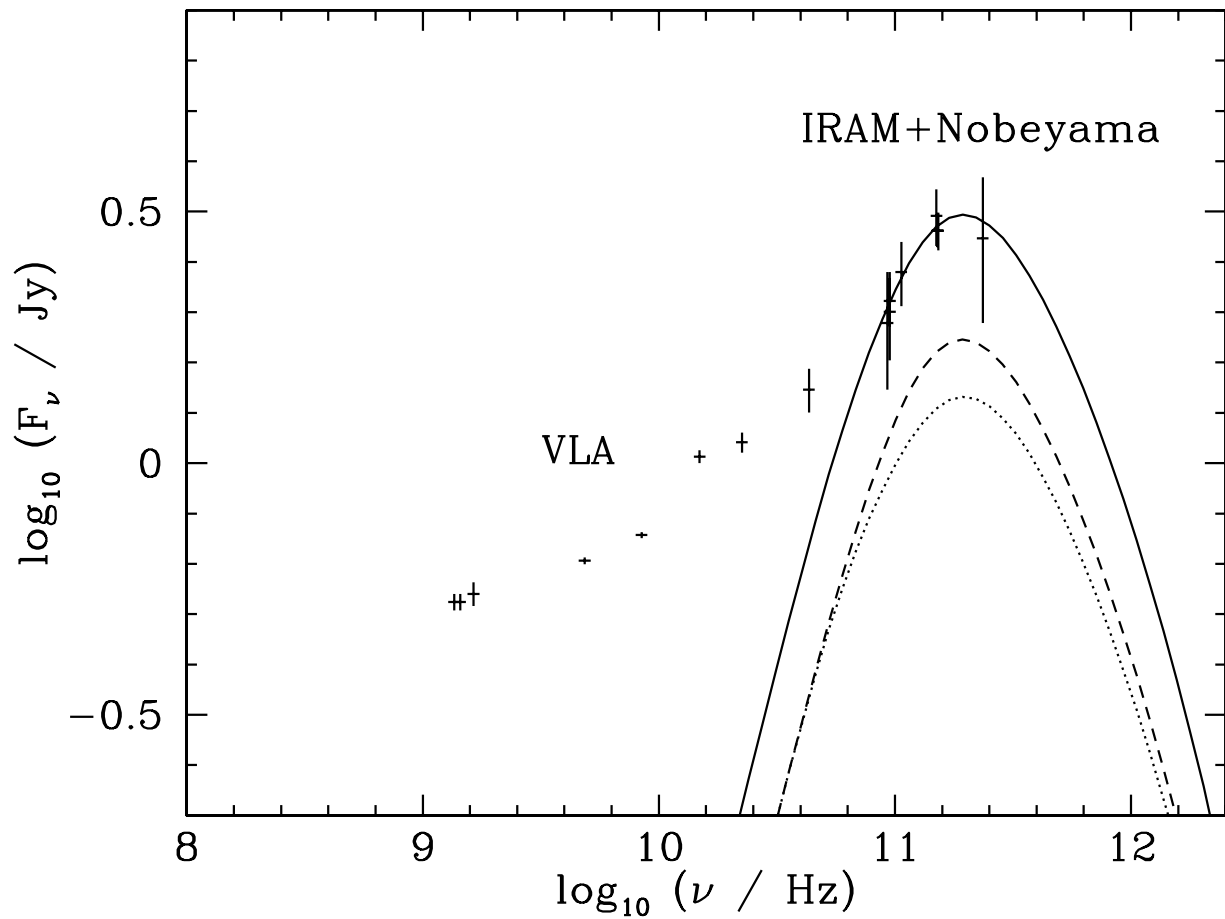


Fig. 7.— Enlargement of the radio portion of the spectrum for the best fit model shown in Figure 1. The values of the parameters are those specified in Figure 1.

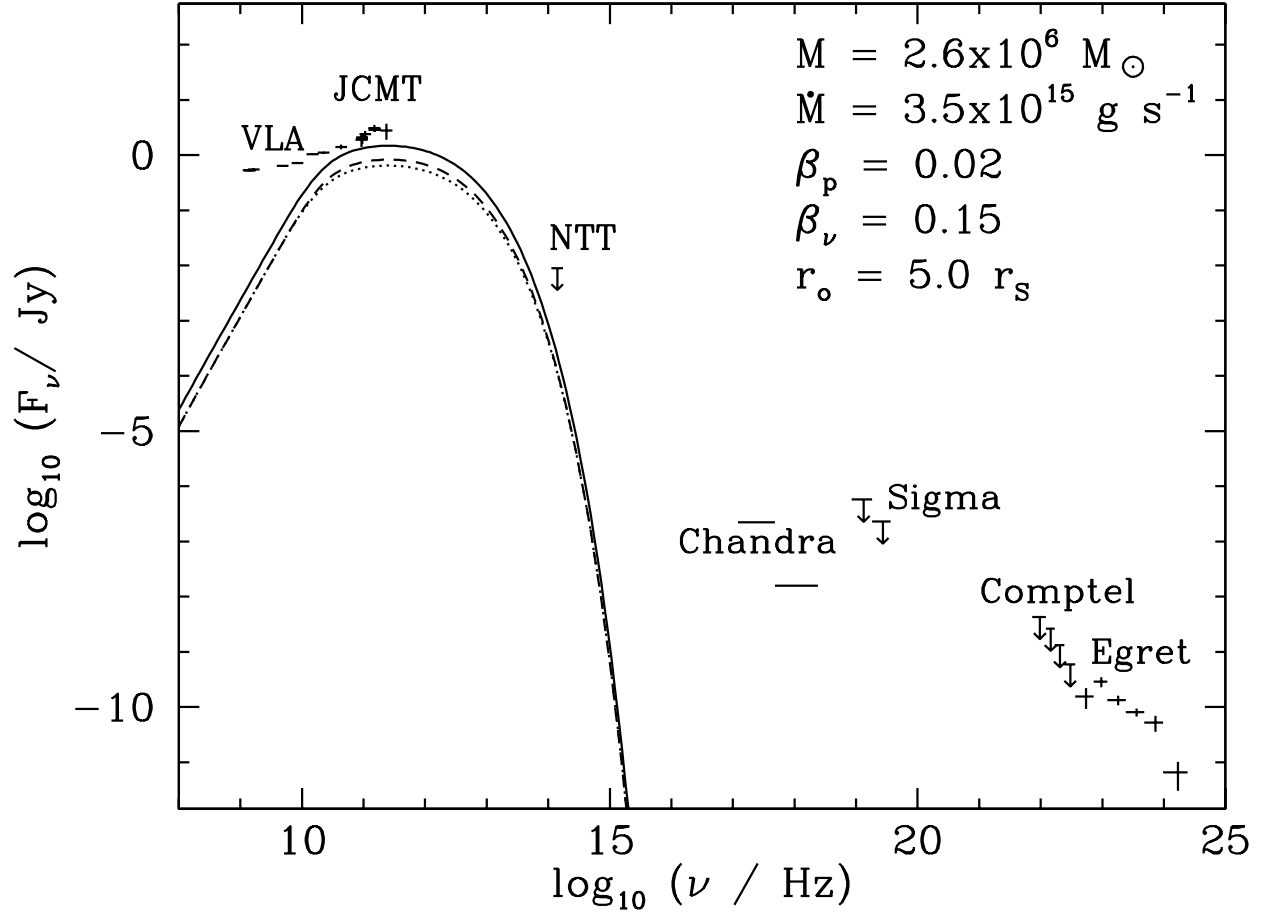


Fig. 8.— Illustration of the effect on the spectrum due to a change in the ratio v_r/v_{ff} at r_0 . In this case, it is 4.0×10^{-3} , compared to a value ten times smaller for the best fit model.

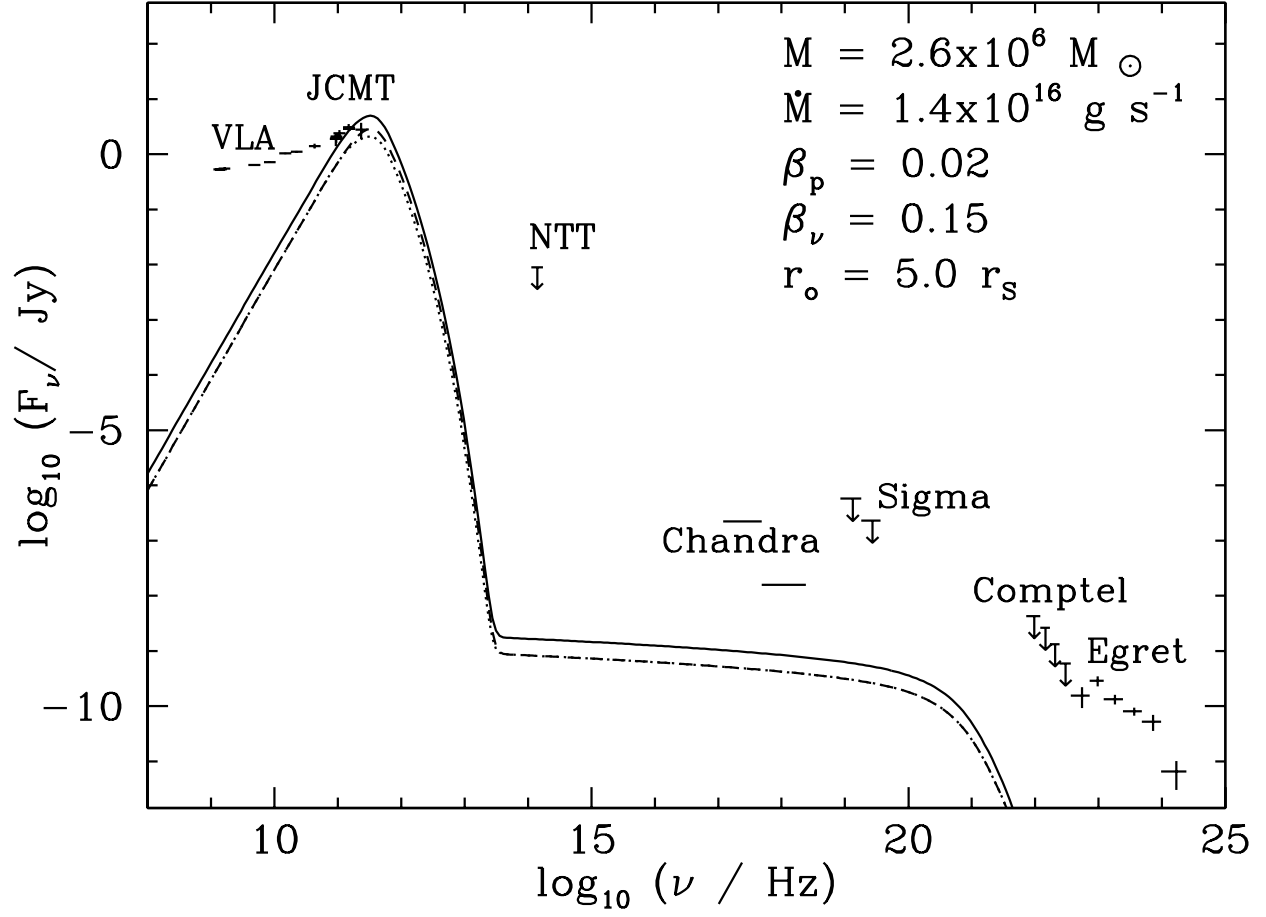


Fig. 9.— Illustration of the effect on the spectrum due to a change in the value of \dot{M} , which is here four times larger than that of the best fit model shown in Figure 1.

To sample the dependence of our fit on the boundary conditions, we show in Figure 8 the spectrum resulting from a Keplerian flow forming with a higher radial velocity at its outer boundary. Equation (70) shows the outer boundary temperature increases by the same order. The implied higher viscosity results in a higher temperature over a more extended range in radii, producing a much flatter “hump” that does not adequately fit the data. However, increasing the accretion rate through this Keplerian region will raise the cooling rate so the gas temperature decreases. But the increased column density results in a spectral bump peaking at higher frequencies than what is observed. In addition, the higher accretion rate would result in a more intense bremsstrahlung emission.

4. Concluding Remarks

Our calculations have shown that under the right conditions, the thermal synchrotron emission from a compact, Keplerian flow around Sgr A* can account for the spectral (sub-mm) bump. Clearly, the peak frequency of this component is correlated to the gas temperature and column density, which characterize several key ingredients, such as the accretion rate and the advected specific angular momentum. The latter appears to be consistent with the values inferred from the large scale Bondi-Hoyle accretion (Coker & Melia 2000), but the required \dot{M} within the circularized region is significantly lower than that expected further out. This contrast probably indicates the need for a gradual mass loss, perhaps in the form of a wind, toward smaller radii. In other words, compared to the value of \dot{M} inferred from the hydrodynamic simulations, the maximum accretion rate permitted by the sub-mm data is several orders of magnitude smaller. Yet the specific angular momentum with which the gas circularizes is not noticeably different from that prescribed by the numerical simulations.

We note that this model would not pass the *Chandra* test (of a very low X-ray

luminosity) if the physical conditions required to produce the sub-mm emission were more extreme than those sampled in this paper. Specifically, the sub-mm and X-ray data would not be mutually consistent within the context of this model if the accretion rate through the Keplerian region was at the Bondi-Hoyle value.

At this point, we can only speculate about what the overall accretion pattern might be like, and we target a future coupling between this analysis and a hydrodynamic simulation of the Keplerian flow merged with the larger scale accretion to address the issue of self-consistency. We anticipate that when the quasi-spherical infall begins to circularize (presumably around $100 - 1000 r_S$), the turbulent mixing of gas elements with high eccentricity readily dissipates the gravitational and kinetic energy densities, raising the internal energy of the gas and possibly leading to a rapid evaporation away from the rotation plane. This expulsion of a wind may cease when the eccentricity reaches a value close to zero, which should occur at a radius $\sim 5 - 10 r_S$. At this point, the flow is very nearly Keplerian, and the dynamo process may become active and efficient, along the lines we have developed in this paper. The spectrum of Sgr A* longward of $1 - 2$ mm is presumably generated within the turbulent mixing (i.e., transition) region.

The first generation of hydrodynamic simulations to address these questions are currently underway and we hope to report the results of this analysis in the very near future.

Acknowledgments This work was supported by a Sir Thomas Lyle Fellowship and a Miegunyah Fellowship for distinguished overseas visitors at the University of Melbourne, and by NASA grants NAG5-8239 and NAG5-9205 at the University of Arizona.

REFERENCES

- Balbus, S.A., Gammie, C.F., and Hawley, J.F. 1994, MNRAS, 271, 197
- Balbus, S.A., & Hawley, J.F. 1991, ApJ, 376, 214 (BH1)
- Balbus, S.A., & Hawley, J.F. 1992, ApJ, 400, 610 (BH2)
- Balick, B. & Brown, RL 1974, ApJ, 194, 265
- Brandenburg, A., Nordlund, Å., & Stein, R. 1995, ApJ, 446, 741 (BNS)
- Coker, R.F., & Melia, F. 2000, ApJ, 534, 723
- Coker, R.F., & Melia, F. 1997, ApJ Letters, 488, L149
- Eckart, A. & Genzel, R. 1996, Nature, 383, 415
- Eckart, A. & Genzel, R. 1997, MNRAS, 284, 576
- Falcke, H., Goss, WM., Matsuo, H., Teuben, P., Zhao, J-H & Zylka, R. 1998, ApJ, 499, 731
- Fleming, T.P., Stone, J.M., & Hawley, J.F. 2000, ApJ, 530, 464
- Genzel, R., Thatte, N., Krabbe, A., Kroker, H. & Tacconi-Garman, LE. 1996, ApJ, 472, 153
- Ghez, AM., Klein, BL., Morris, M. & Becklin, EE. 1998, ApJ, 509, 678
- Hawley, J.F., 2000, ApJ, 528, 462
- Hawley, J.F., & Balbus, S.A. 1991, ApJ, 376, 223 (HB1)
- Hawley, J.F., & Balbus, S.A. 1992, ApJ, 400, 595 (HB2)
- Hawley, J.F., Gammie, C.F., & Balbus, S.A. 1995, ApJ, 440, 742 (HGB1)
- Hawley, J.F., Gammie, C.F., & Balbus, S.A. 1996, ApJ, 464, 690 (HGB2)

- Ipsier, J.R. & Price, R.H. 1977, ApJ, 216, 578.
- Jin, L. 1996, ApJ, 457, 798
- Kowalenko, V. & Melia, F. 1999, MNRAS, 310, 1053
- Melia, F. 1992, ApJ Letters, 387, L25.
- Melia, F. 1994, ApJ, 426, 577
- Melia, F., Jokipii, J.R. & Narayanan, A. 1994, ApJ Letters, 395, 87
- Pacholczyk, A.G. 1970, Radio Astrophysics, (W.H. Freeman and Company: San Francisco)
- Petschek, H.E. 1964, Proc. of the Symposium on Physics of Solar Flares (NASA SP-50), 425.
- Shapiro, S.L. 1973, ApJ, 185, 69.
- Spitzer, Lyman, Jr. 1961, Physics of Fully Ionized Gases, (John Wiley & Sons: New York)
- Stoeger, W.R. 1980, ApJ, 235, 216
- Stone, J.M., Hawley, J.F., Gammie, C.F., & Balbus, S.A. 1996, ApJ, 463, 656 (SHGB)
- van Hoven, G. 1979, ApJ, 232, 572.
- Zylka, R., Mezger, P.G. & Lesch, H. 1992, AA, 261, 119
- Zylka, R., Mezger, P.G., Ward-Thompson, D., Duschl, W.J. & Lesch, H. 1995, AA, 297, 83